Chinese Journal of Natural Medicines

Bioactivity-guided discovery of antiviral templichalasins AC from the endophytic fungus *Aspergillus templicola*

Teng Cai, Jingzu Sun, Wenxuan Chen, Qiang He, Baosong Chen, Yulong He, Peng Zhang, Yanhong Wei, Hongwei Liu, Xiaofeng Cai

Citation: Teng Cai, Jingzu Sun, Wenxuan Chen, Qiang He, Baosong Chen, Yulong He, Peng Zhang, Yanhong Wei, Hongwei Liu, Xiaofeng Cai, Bioactivity-guided discovery of antiviral templichalasins AC from the endophytic fungus *Aspergillus templicola*, Chinese Journal of Natural Medicines, 2025, 23(6), 754-761. doi: 10.1016/S1875-5364(25)60880-6.

View online: https://doi.org/10.1016/S1875-5364(25)60880-6

Chinese Journal of Natural Medicines 23 (2025) 754-761

Contents lists available at ScienceDirect

Chinese Journal of Natural Medicines

journal homepage: www.cjnmcpu.com/

Original article

Bioactivity-guided discovery of antiviral templichalasins A–C from the endophytic fungus *Aspergillus templicola*

Teng Cai[a,Δ], Jingzu Sun[c,Δ], Wenxuan Chen[d], Qiang He[e], Baosong Chen[c], Yulong He[a], Peng Zhang[a], Yanhong Wei[d], Hongwei Liu[c,*], Xiaofeng Cai[a,b,*]

[a] *Hubei Key Laboratory of Natural Medicinal Chemistry and Resource Evaluation, School of Pharmacy, Tongji Medical College, Huazhong University of Science and Technology, Wuhan 430030, China*

[b] *State Key Laboratory of Dao-di Herbs, National Resource Center for Chinese Materia Medica, China Academy of Chinese Medical Sciences, Beijing 100700, China*

[c] *State Key Laboratory of Mycology, Institute of Microbiology, Chinese Academy of Sciences, Beijing 100101, China*

[d] *Sino-German Biomedical Center, Key Laboratory of Fermentation Engineering (Ministry of Education), Hubei University of Technology, Wuhan 430068, China*

[e] *Institute of Food Inspection, Xianning Public Inspection and Testing Center of Hubei Province, Xianning 437000, China*

ARTICLE INFO

Article history:
Received 18 July 2024
Revised 11 September 2024
Accepted 1 November 2024
Available online 20 July 2025

Keywords:
Aspergillus templicola
Aspochalasins
Structural elucidation
Antiviral activity

ABSTRACT

The bioactivity-guided isolation of potentially active natural products has been widely utilized in pharmaceutical discovery. In this study, by screening fungal extracts against coxsackievirus B3 (CVB3), three new aspochalasins, templichalasins A–C (**1**–**3**), along with six known aspochalasins (**4**–**9**) were isolated from an active extract derived from the endophytic fungus *Aspergillus templicola* LHWf045. Compound **1** features a unique 5/6/5/7/5 pentacyclic ring system, while compounds **2** and **3** possess unusual 5/6/6/7 tetracyclic skeletons. Their structures were characterized through extensive spectroscopic analyses, electronic circular dichroism (ECD) calculations, and single-crystal X-ray diffraction analysis. Additionally, we demonstrated that compound **4** can be readily converted into compounds **1**–**3** under mild acidic conditions and proposed a plausible mechanism for this conversion. Bioactivity evaluation of compounds **1**–**9** against CVB3 revealed the inhibitory effects of all compounds against the virus. Notably, compound **9** exhibited superior antiviral activity, surpassing the commercial drug ribavirin in selectivity index (SI) value.

1. Introduction

Coxsackievirus B3 (CVB3), a prevalent pathogen within the picornavirus family, poses a significant public health threat due to its association with various diseases, such as myocarditis, pancreatitis, and aseptic meningitis [1-3]. Despite the prevalence and severity of CVB3-related illnesses, no approved drugs specifically target CVB3 infection [4]. Although several candidates have shown potential in inhibiting CVB3 in recent decades, all of them have exhibited adverse side effects or insufficient antiviral efficacy, hindering their final market approval [5, 6]. Thus, there is an urgent need to discover novel and effective antiviral drug candidates against CVB3. *Aspergillus* species are remarkable microorganisms capable of producing numerous natural products with diverse structures and significant biological activities, rendering them an inexhaustible and promising source of new antiviral agents [7, 8]. In our continuous endeavors to explore these microbes, *Aspergillus templicola* LHWf045 (LHWf045), an endophytic fungus isolated from the medicinal plant *Curcuma aromatica* Salisb, showed antiviral activity against CVB3 during preliminary screening. The crude extract obtained from rice fermented with LHWf045 exhibited promising inhibitory activity against CVB3 upon infection. As LHWf045 represents a new medicinal plant endophyte, with limited literature available on its secondary metabolites, it was selected for further investigation to identify potential antiviral candidates.

Cytochalasans constitute a large group (> 500 isolated compounds) of fungal natural products, characterized by an isoindole moiety fused to a macrocyclic ring [9, 10]. Among them, aspochalasins are the third-largest subgroup, distinguished by the presence of a leucine residue [9]. Recent advancements in the identification of biosynthetic gene clusters have provided insights into their hybrid polyketide synthase (PKS)-nonribosomal peptide synthetase (NRPS) hybrid pathways [11]. Nevertheless, certain polycyclic cytochalasans with complex, polymerized scaffolds have been identified as acid-mediated artifacts of monocytochalasans, highlighting the acid sensitivity within the cytochalasan family and emphasizing the need for caution when handling these compounds [10-13]. Moreover, cytochalasans exhibit a wide range of bioactivities, including antimicrobial, cytotoxicity, anti-HIV, and immunoregulatory effects [14]. Despite the extensive biological diversity of cytochalasans reported in previous studies [14], their potential antiviral properties, particularly against CVB3, remain unexplored, suggesting that cytochalasans may hold untapped potential as novel antiviral agents.

The bioactivity-guided isolation of active natural products has been widely utilized to accelerate the pharmaceutical discovery process. Preliminary bioassay results revealed that the crude

* Corresponding author.
E-mail addresses: liuhw@im.ac.cn (H. Liu); caixiaofeng@hust.edu.cn (X. Cai)
Δ These authors contributed equally to this work.

https://doi.org/10.1016/S1875-5364(25)60880-6

extract of LHWf045 displayed promising inhibitory activity against CVB3, warranting further investigation for potential anti-CVB3 compounds. Thus, three new aspochalasins: templichalasins A–C (**1**–**3**), along with six known aspochalasins (**4**–**9**), were isolated and identified (Fig. 1). Compound **1** represents a new 5/6/5/7/5 pentacyclic skeleton, while compounds **2** and **3** possess rare 5/6/6/7 tetracyclic scaffolds. Furthermore, we demonstrated that compound **4** exhibited high sensitivity to acid, leading to the formation of compounds **1**–**3**, possibly attributable to the presence of its unstable *α*,*β*-unsaturated ketone moiety. Compounds **1**–**8** displayed moderate antiviral effects on CVB3, with SI values ranging from 1.13 to 3.71, whereas compound **9** (SI = 16.08) showed superior antiviral activity against CVB3 compared to commercial ribavirin (SI = 7.89). This study presents the isolation, structure elucidation, and antiviral evaluation of compounds **1**–**9**.

2. Results and discussion

The endophytic fungus LHWf045-fermented rice was extracted with ethyl acetate (EA). The resulting crude extract exhibited significant antiviral activity against CVB3, demonstrating an inhibitory ratio of 70%–80% at a concentration of 50 μg·mL^{-1}. This observation indicated the potential presence of antiviral agents within the EA extract. Subsequent isolation and analysis of the active extract led to the identification of nine compounds, including three new aspochalasins, templichalasins A–C (**1**–**3**), alongside six known ones (**4**–**9**) (Fig. 1).

Templichalasin A (**1**) presented as a colorless crystal with prominent ion peaks at *m/z* 400.2512 [M + H]$^+$ and 799.4936 [2M + H]$^+$ in high-resolution electrospray ionization mass spectrometry (HR-ESI-MS) under positive ionization mode. In conjunction with the analysis of its ^{13}C NMR data, the molecular formula of compound **1** was deduced to be $C_{24}H_{33}NO_4$, indicating nine degrees of unsaturation. Analysis of the ^{1}H nuclear magnetic resonance (NMR) (Table 1) and heteronuclear single quantum coherence (HSQC) spectra of compound **1** revealed the presence of five methyl groups (δ_H 1.78, s; 1.31, s; 1.21, d, J = 7.0 Hz; 0.93, d, J = 6.4 Hz; and 0.91, d, J = 6.4 Hz), one oxygenated methine (δ_H 4.46, dd, J = 10.1, 5.6 Hz), one olefinic proton (δ_H 5.79, br s), and one exchangeable proton (δ_H 6.34, br s). Further examination of the ^{13}C NMR (Table 2) and distortionless enhancement by polarization transfer (DEPT) spectra revealed 24 carbon signals, comprising two ketone carbonyls (δ_C 212.4 and 212.1), one amide carbonyl (δ_C 173.9), one double bond (δ_C 141.8 and 122.6), two quaternary carbons (δ_C 83.8 and 68.9) including an oxygenated one (δ_C 83.8), eight methines (including an oxygenated methine at δ_C 84.1), four methylenes, and five methyl groups. This combination of structural features suggested that compound **1** belongs to the aspochalasin subfamily of cytochalasans.

A detailed comparison of the 1D NMR data between compound **1** and flavichalasine D revealed significant similarities, suggesting a structural resemblance [15]. However, notable differences were observed in the chemical shift values of C-13 (δ_C 46.1 in **1**; δ_C 39.3 in flavichalasine D), C-19 (δ_C 41.0 in **1**; δ_C 53.6 in flavichalasine D), and C-20 (δ_C 47.5 in **1**; δ_C 72.7 in flavichalasine D) [15]. This observation implies that compound **1** shares the same isoindolone moiety as flavichalasine D [15], with structural variations likely occurring within the macrocyclic ring. The presence of an oxygen bridge between C-14 and C-17 in compound **1** was deduced from the chemical shift values of C-14 (δ_C 83.8) and C-17 (δ_C 84.1), along with the heteronuclear multiple bond correlation (HMBC) (Fig. 2) observed from H-17 to C-14. The position of the oxygen bridge aligns with that in flavichalasine D [15]. However, the proton spin systems of H-7/H-8/H-13/H-20/H_2-19 in the ^{1}H–^{1}H COSY spectrum, together with the HMBC correlations from H-13 to C-19 and from H_2-20 to C-14, confirmed the formation of a new C-C bond between C-13 and C-20 in compound **1**. The establishment of this bond results in a previously unreported fused polycyclic architecture, characterized by a 5/6/5/7/5 ring fusion pattern, which is distinguishable from the 5/6/6/6/5 system characteristic of flavichalasine D [15].

The relative configuration of compound **1** was elucidated through a comprehensive analysis of its NOESY spectrum. An examination of the observed NOESY correlations (Fig. 2) revealed that the relative configuration of the isoindolone moiety in compound **1** aligns with that of flavichalasine D [15]. Nuclear Overhauser effect spectroscopy (NOESY) correlations of H-8/CH_3-25, H-8/H-20, and H-20/CH_3-25 indicated the *β*-orientation of both H-8 and H-20. Further analysis revealed NOESY correlations of H-7/H-13, H-7/H-15a, H-13/H-15a, H-13/H-16b, and H-16a/H-17, suggesting the *α*-orientation of H-13 and the *β*-orientation of the oxygen bridge.

Compound **1** was successfully crystalized through slow evaporation from a 98% methanol–water solution. However, the relatively large Flack parameter of −0.18(11) precluded definitive determination of the absolute configuration (Fig. S3). To resolve this stereochemical ambiguity, the experimental electronic circular dichroism (ECD) spectrum of compound **1** was compared with its calculated ECD spectrum (Fig. 3). The observed excellent agreement between the experimental and calculated spectra allowed for the unambiguous assignment of the absolute configuration of compound **1** as 3*S*,4*R*,5*S*,8*R*,9*S*,13*R*,14*S*,17*R*,20*S*.

Templichalasin B (**2**) was obtained as a white amorphous

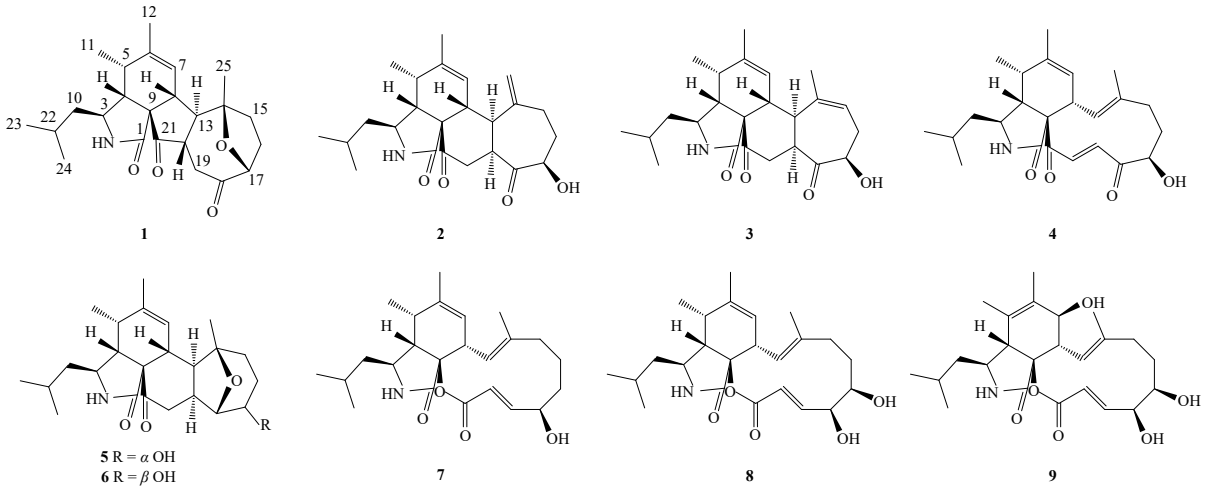

Fig. 1 Structures of compounds **1**–**9**.

Table 1 ^{1}H NMR spectroscopic data of compounds **1**–**3** (*J* in Hz).

No.	δ_H **1** ($CDCl_3$) [a]	δ_H **2** ($CDCl_3$) [a]	δ_H **2** (CD_3OD) [b]	δ_H **3** ($CDCl_3$) [a]	δ_H **3** (CD_3OD) [a]
2	6.34, br s	5.83, br s		5.97, br s	
3	3.28, m	3.17, m	3.22, ddd (9.4, 4.7, 2.8)	3.13, m	3.19, ddd (9.3, 4.7, 2.8)
4	2.37, m	3.03, dd (5.6, 2.9)	2.89, dd (5.6, 2.8)	2.94, dd (5.6, 2.9)	2.82, dd (5.6, 2.8)
5	2.43, m	2.31, m	2.34, m	2.20, m	2.23, m
7	5.79, br s	5.48, br s	5.48, br s	5.47, br s	5.52, br s
8	2.49, m	2.20, m	2.32, m	2.25, br d (12.6)	2.35, m
10a	1.54, m	1.54, m	1.50, ddd (13.9, 9.4, 4.7)	1.53, m	1.50, ddd (13.8, 9.3, 4.7)
10b	1.31, m	1.32, m	1.31, ddd (13.9, 9.4, 4.7)	1.29, m	1.29, ddd (13.8, 9.3, 4.7)
11	1.21, d (7.0)	1.17, d (7.2)	1.21, d (7.2)	1.13, d (7.2)	1.19, d (7.2)
12	1.78, s	1.71, s	1.73, s	1.72, s	1.74, s
13	3.69, dd (12.2, 10.1)	4.33, m	4.26, dd (12.4, 5.1)	4.39, dd (12.6, 4.2)	4.33, dd (12.6, 4.1)
15a	2.05, dd (11.5, 8.2)	2.20, m	2.22, m	5.76, dd (9.6, 3.6)	5.80, dd (9.3, 3.0)
15b	1.71, m	1.76, m	1.82, m		
16a	2.52, m	2.11, m	2.18, m	2.43, ddd (14.5, 9.6, 4.6)	2.32, m
16b	2.23, m		1.99, m	1.82, m	1.86, m
17	4.46, dd (10.1, 5.6)	4.32, m	4.40, m	4.11, dd (11.6, 4.6)	4.17, dd (11.7, 4.4)
19a	2.95, m	3.63, td (5.1, 3.1)	3.68, td (5.1, 3.2)	3.32, m	3.44, m
19b	2.69, dd (17.4, 9.9)				
20a	2.98, m	3.14, dd (14.8, 5.1)	3.00, dd (15.0, 5.1)	3.10, dd (14.6, 5.0)	2.97, dd (14.8, 4.9)
20b		2.54, dd (14.8, 3.1)	2.50, dd (15.0, 3.2)	2.82, dd (14.6, 2.5)	2.71, dd (14.8, 2.4)
22	1.52, m	1.54, m	1.64, m	1.50, m	1.63, m
23	0.91, d (6.4)	0.91, d (6.3)	0.93, d (6.5)	0.90, d (6.3)	0.93, d (6.5)
24	0.93, d (6.4)	0.92, d (6.3)	0.94, d (6.5)	0.91, d (6.3)	0.94, d (6.5)
25	1.31, s	5.02, m	5.01, m	2.03, s	2.03, s

[a] Recorded at 400 MHz; [b] Recorded at 600 MHz.

powder, with ion peaks at *m/z* 400.2519 $[M + H]^+$ and 799.4926 $[2M + H]^+$ in HR-ESI-MS under positive ionization mode, suggesting a molecular formula of $C_{24}H_{33}NO_4$ with nine degrees of unsaturation. Although compound **2** shares the same molecular formula as compound **1**, its markedly different retention time on liquid chromatography (LC) suggests that it is a structural isomer. Analysis of the 1D NMR data (Tables 1 and 2) of compound **2** ($C_{24}H_{33}NO_4$) revealed a strong resemblance to the tetracyclic (5/6/6/7) aspochalasin flavichalasine A ($C_{24}H_{33}NO_5$), suggesting a similar planar structure but with the absence of one hydroxyl group [15]. This inference was further supported by 2D NMR data (DEPT and HSQC spectra), which indicated the replacement of an oxygenated methine—present in flavichalasine A—with an additional non-oxygenated methylene group in compound **2** [15]. This observation indicated the reduction of the oxygenated methine at C-20 in flavichalasine A to a methylene (C-20, δ_C 40.4; H_2-20, δ_H 3.14 and 2.54) in compound **2** [15]. This structural modification was further supported by the ^{1}H–^{1}H COSY correlation between H-19 and H_2-20, and the HMBCs between from H_2-20 to C-9, C-18, and C-21 in compound **2**, thus confirming its planar structure (Fig. 2). The absence of the NOESY correlation between H-8 and H-19 observed in flavichalasine A [15], along with the emergence of NOESY correlations of H-13/H-19, H-13/H-16a, H-16a/H-19, and H-17/H-19 in compound **2**, indicated the *α*-orientation of both H-17 and H-19, thereby establishing the relative configuration of compound **2** (Fig. 2). Finally, the absolute configuration of compound **2** was determined to be 3*S*,4*R*,5*S*,8*R*,9*S*,13*R*,17*R*,19*S* through ECD calculations (Fig. 3).

Templichalasin C (**3**) exhibited the same molecular weight and similar retention time in LC as compound **2**, suggesting an identical skeleton. Analysis of the 1D and 2D NMR data of compound **3** revealed the presence of an additional methyl (C-25, δ_C 29.2; CH_3-25, δ_H 2.03) and signals corresponding to a trisubstituted double bond (C-14, δ_C 142.5; C-15, δ_C 122.1; H-15, δ_H 5.76), while lacking the terminal double bond and a methylene group observed in compound **2** (Tables 1 and 2). This observation indicated the isomerization of the double bond from the exocyclic position (between C-14 and C-25) in compound **2** to an endocyclic position (between C-14 and C-15) in compound **3**. The location of the double bond between C-14 and C-15 in compound **3** was further supported by HMBCs from CH_3-25 to C-13, C-14, and C-15, as well as from H-13 and H-17 to C-15 (Fig. 2). Considering the biosynthetic origins, the relative configurations at C-3, C-4, C-5, C-8, C-9, C-13, C-17, and C-19 in compound **3** were expected to be consistent with that of compound **2**. This assumption was corroborated by the presence of NOESY correlations of H-7/H-13, H-

Table 2 ^{13}C NMR spectroscopic data of compounds **1**–**3**.

No.	δ_C **1** ($CDCl_3$) [a]	δ_C **2** ($CDCl_3$) [a]	δ_C **2** (CD_3OD) [b]	δ_C **3** ($CDCl_3$) [a]	δ_C **3** (CD_3OD) [a]
1	173.9	174.0	175.9	173.8	175.8
3	50.9	51.6	52.9	51.4	52.8
4	47.7	48.1	49.6	48.0	49.6
5	36.1	35.1	36.2	34.7	35.9
6	141.8	140.4	141.5	141.6	142.6
7	122.6	123.6	124.9	122.7	123.9
8	44.3	39.1	40.1	40.4	41.2
9	68.9	66.4	68.0	66.5	68.2
10	48.2	47.1	48.6	47.1	48.6
11	13.7	13.4	13.8	13.4	13.8
12	20.2	20.2	20.1	20.3	20.1
13	46.1	41.5	42.7	38.5	39.7
14	83.8	148.8	150.9	142.5	143.7
15	40.6	28.9	29.9	122.1	123.0
16	29.7	32.4	33.7	33.1	33.7
17	84.1	76.3	77.2	75.8	76.9
18	212.4	214.3	215.2	213.5	214.5
19	41.0	48.1	49.4	50.7	52.0
20	47.5	40.4	41.6	41.4	42.7
21	212.1	204.0	207.0	203.3	206.4
22	24.8	25.3	25.7	25.2	25.7
23	21.9	21.7	22.1	21.6	22.1
24	23.4	23.7	24.0	23.7	24.0
25	20.7	116.4	116.1	29.2	29.3

[a] Recorded at 100 MHz; [b] Recorded at 150 MHz.

13/H-19, and H-17/H-19 of compound **3**, further confirming the identical relative configuration to compound **2** (Fig. 2). Ultimately, the absolute configuration of compound **3** was determined as 3*S*,4*R*,5*S*,8*R*,9*S*,13*R*,17*R*,19*S* through ECD calculations (Fig. 3).

In addition to the newly characterized compounds, six known analogs (**4**–**9**) were identified by comparison of their HR-ESI-MS and NMR data with those reported previously (Figs. S53–S79) [16-19].

3. Acid-mediated intramolecular cycloaddition

LC-HR-MS analysis of the EA crude extract identified compound **4** as a major constituent, easily separable through standard techniques (Fig. 4, i–v). In contrast, compounds **1**–**3** were detected as trace levels, presenting significant challenges for purification in preparative quantities (Fig. 4, i–v). Nevertheless, these minor metabolites were successfully isolated and structurally characterized, prompting consideration of their possible origin as non-native products formed during the isolation process. The isolation yields of compounds **1**–**3** ranged from 7.2 to 28.3 mg, whereas only 16.4 mg of compound **4** was obtained. This variation suggested chemical conversion during the isolation process, leading to the depletion of compound **4** and the concurrent formation of compounds **1**–**3**. This hypothesis is supported by previous reports demonstrating that polycyclic cytochalasans, particularly those possessing 5/6/5/8 tetracyclic, 5/6/6/7/5 pentacyclic, and 5/6/6/5/6 pentacyclic skeletons, may not be genuine natural products but rather artifacts derived from macrocyclic cytochalasans under acidic conditions [10-13]. Given that compounds **1**–**3** possess stable tetracyclic and pentacyclic scaffolds, while compound **4** is a macrocyclic aspochalasin containing an unstable *α*,*β*-unsaturated ketone moiety within its macrocyclic ring, it is proposed that compounds **1**–**3** originate from compound **4** *via* non-enzymatic, acid-catalyzed conversions. Two plausible mechanistic pathways are proposed for this conversion (Fig. 5). In path A, the protonation of the C-18 carbonyl group could trigger a new C–C bond formation between C-13 and C-20. The resulting carbocation at C-14 would subsequently be quenched by the hydroxyl group at C-17, leading to the formation of compound **1**. Alternatively, in path B, the protonation of the C-21 carbonyl might induce C–C bond formation between C-13 and C-19, accompanied by carbocation generation at C-14.

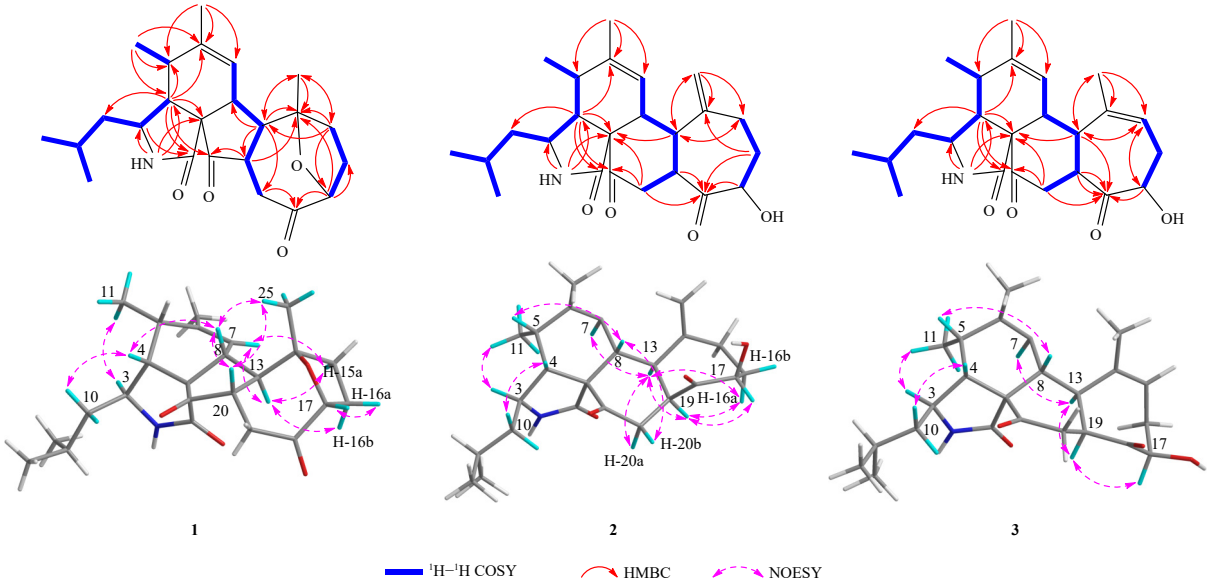

Fig. 2 ^{1}H–^{1}H COSY, HMBC, and NOESY correlations of compounds **1**–**3**.

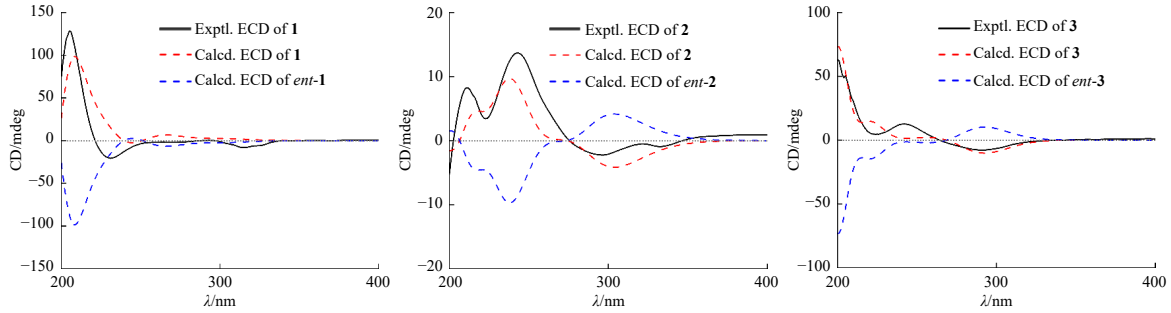

Fig. 3 Experimental and calculated ECD curves of compounds **1**–**3**.

Subsequent *β*-eliminations at C-25 or C-14 would afford compound **2** or **3**, respectively.

To validate this hypothesis, compound **4** (50 μg) was treated with 200 μL each of TFA/MeOH and TFA/H_2O solutions at varying concentrations (1%, 10%, and 30%) and allowed to react at room temperature for 24 h. Subsequently, 10 μL of the reaction mixture underwent LC-HR-MS analysis. The results confirmed that compound **4** could indeed convert into compounds **1**–**3** under acidic conditions (Fig. 4, vi–xi). Furthermore, the efficiency of this conversion increased gradually with higher TFA concentrations, with complete conversion of compound **4** to compounds **1**–**3** observed when treated with 10% TFA/MeOH and 30% TFA/H_2O (Fig. 4, vi–xi). The observed acid-catalyzed intramolecular cyclization reaction is noteworthy, offering a rapid and efficient pathway for generating complex polycyclic frameworks, thereby expanding the structural diversity of cytochalasans. Additionally, it corroborates the structures of compounds **1**–**3**.

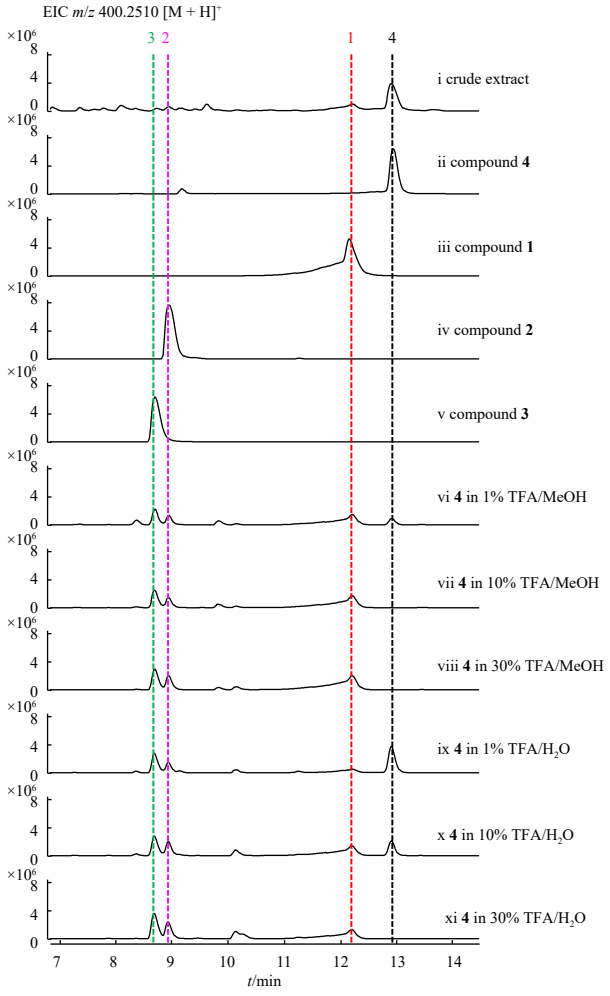

Fig. 4 LC-MS analysis of the EA crude extract and acid-mediated conversion products of compound **4**. The extracted ion chromatograms (EICs) were extracted at *m/z* 400.2510 [M + H]$^+$.

4. Antiviral activities of 1–9 against CVB3

Compounds **1**–**9** underwent cytotoxicity testing against Hep-2 (human laryngeal epithelial cancer) cells and antiviral activity against CVB3 in a cell-based assay, with ribavirin as the positive control. Table 3 summarizes the relevant activity results, including the half-maximal cytotoxic concentration (CC_{50}), half-maximal effective concentration (EC_{50}), and selectivity index (SI) values. Compounds **4**, **7**, and **8** exhibited high cytotoxicity against the Hep-2 cells, with CC_{50} values of 37.5, 37.5, and 18.75 μmol·L^{-1}, respectively, while compounds **1**–**3**, **5**, **6**, and **9** demonstrated low cytotoxicity, with CC_{50} values ranging from 150 to 250 μmol·L^{-1} (Table 3, Fig. S4). Additionally, all tested compounds displayed good inhibitory activity against CVB3, with EC_{50} values ranging from 8.42 to 133.33 μmol·L^{-1} (Table 3, Fig. S5). Notably, compound **9** exhibited superior antiviral activity, surpassing the commercial drug ribavirin in SI value (Table 3).

Due to the significant cytopathic effects (CPEs) induced by CVB3 infection, we indirectly evaluated the antiviral activity of these compounds by analyzing CPEs in CVB3-infected Hep-2 cells. Fig. S6 illustrates the inhibitory effects of all tested compounds on virus-induced CPEs. In the absence of tested compounds, virus-infected cells exhibited rounded morphology and detachment from the culture dish. However, treatment with 25 μmol·L^{-1} of compound **9** almost completely prevented virus-induced CPEs (Fig. S6). These results suggested that virus infection induces substantial CPEs in host cells, and compound **9** significantly alleviates this effect, indirectly reflecting its potent inhibitory effect on virus infection.

Given the potent antiviral activity of compound **9** against CVB3, further investigations were conducted to assess its effect on virus progeny yield. The CVB3 virus progeny titers were significantly reduced by approximately 2.5 log after being treated with 50 μmol·L^{-1} of compound **9** compared to the untreated control group. These findings indicate that compound **9** effectively inhibits virus proliferation in host cells.

5. Conclusions

In this study, we conducted an antiviral-guided chemical investigation of the crude extract from the endophytic fungus LH-Wf045, leading to the discovery of three new aspochalasins, templichalasins A–C (**1**–**3**), along with six known aspochalasins (**4**–**9**). Compound **1** features an unprecedented 5/6/5/7/5 pentacyclic scaffold, while compounds **2** and **3** possess rare 5/6/6/7 tetracyclic skeletons. Moreover, this study demonstrates that compounds **1**–**3** are acid-mediated transformation products of compound **4** and proposes plausible mechanisms for these conversions. Bioactivity assessment reveals that compound **9** exhib-

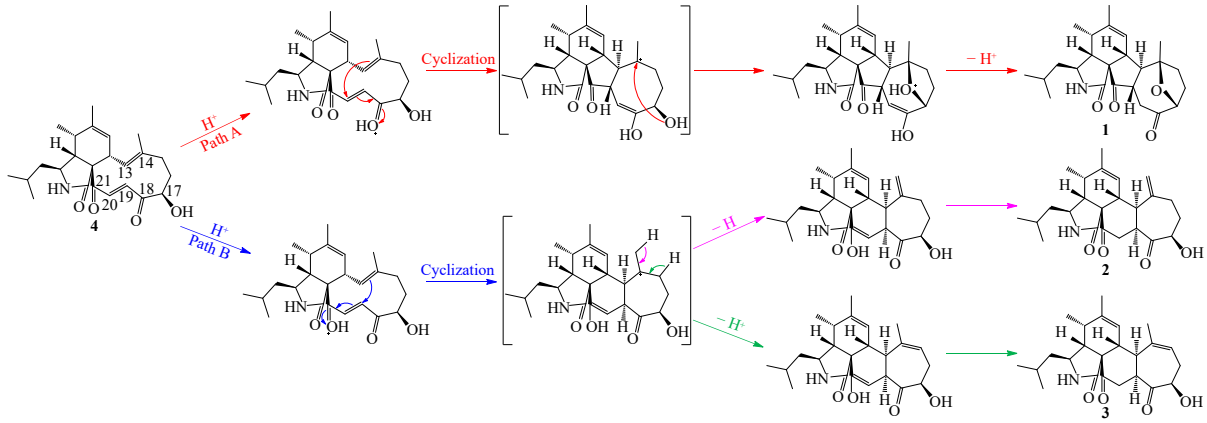

Fig. 5 The proposed mechanism of conversion of **4** to **1**–**3** *via* protonation of the carbonyl groups under acidic conditions.

its considerable inhibitory activity against CVB3, with the highest SI value of 16.08 among all tested compounds. These findings significantly contribute to expanding the chemical and pharmacological diversity of aspochalasins.

6. Experimental

6.1. General experimental procedures

Optical rotations were measured in methanol using a Rudolph Autopol IV automatic polarimeter (Rudolph Research Analytical, Hackettstown, NJ, USA) with sodium light (589 nm). UV spectra were recorded on a PerkinElmer Lambda 35 spectrophotometer (PerkinElmer, Inc., Waltham, MA, USA). IR spectra were detected using a Thermo Scientific Nicolet iS50R FT-IR spectrophotometer (Thermo Fisher Scientific Inc., Waltham, MA, USA). Circular dichroism spectra were acquired with a JASCO-810 instrument (JASCO Co., Ltd., Tokyo, Japan). Semi-preparative high-performance liquid chromatography (HPLC) was performed by employing an Agilent Technologies 1260 Infinity system (Agilent Technologies, Inc., Santa Clara, CA, USA) equipped with a YMC-Pack ODS-A RP-18 column (250 mm × 10 mm, 5 μm, YMC Co., Ltd., Kyoto, Japan). HR-ESI-MS data were acquired using an Agilent 1290 Infinity II/6545 QTOF LC-MS with an Agilent Proshell 120 EC-C_{18} column (2.7 μm, 150 mm × 3.0 mm). NMR spectra were obtained using Bruker AM-400 and AVANCE NEO 600 spectrometers (Bruker, Karlsruhe, Germany), with tetramethylsilane (TMS) as the internal standard. Crystallographic data were collected on an XtaLAB PRO MM007HF diffractometer (Rigaku) with Cu Kα radiation. Column chromatography was performed on silica gel (100–200 or 200–300 mesh, Qingdao Marine Chemical Inc., Qingdao, China) and Sephadex LH-20 (Cytiva Sweden AB, Uppsala, Sweden). Fractions and purified compounds were monitored by TLC (silica gel $HSGF_{254}$, Yantai Jiangyou Silica Gel Development Co., Ltd., Yantai, China), and the spots on silica gel plates were visualized by heating after spraying with 10% H_2SO_4 in ethanol (*V*/*V*).

Table 3 Cytotoxicity and antiviral activity of compounds **1**–**9** against coxsackievirus B3 (CVB3).

Compound No.	[a] CC_{50}/(μmol·L^{-1})	[b] EC_{50}/(μmol·L^{-1})	[c] SI
1	150.00	40.33	3.71
2	150.00	133.33	1.13
3	150.00	83.33	1.80
4	37.50	10.42	3.60
5	150.00	75.00	2.00
6	250.00	108.33	2.30
7	37.50	12.17	3.08
8	18.75	8.42	2.23
9	150.00	9.33	16.08
[d] Ribavirin	965.00	122.30	7.89

[a] CC_{50}: compound concentration required to reduce cell viability by 50%; [b] EC_{50}: compound concentration required to achieve 50% protection from virus-induced cytopathogenicity; [c] SI (selectivity index): ratio by CC_{50}/EC_{50}; [d] Ribavirin, used as a positive control.

6.2. Fungal material

The fungal strain *Aspergillus templicola* LHWf045 was isolated from *Curcuma aromatica* Salisb collected at 116°25'E, 39°47'N, Nanning, Guangxi, China. The strain was identified through rDNA-ITS sequence analysis, with the GenBank accession No. PP658056.

6.3. Fermentation, extraction, and isolation

The strain was cultivated on potato dextrose agar (PDA) plates at 28 °C for 7 d to prepare the seed culture. The fully colonized PDA was then aseptically fragmented into uniform blocks and used to inoculate eight autoclaved 1 L Erlenmeyer flasks, each containing 150 g of sterile rice (dry weight) and 190 mL of double-distilled water (dd H_2O). The inoculated flasks were incubated at 28 °C for 20 d to facilitate solid-state fermentation. Following fermentation, the entire rice substrate from each flask was subjected to three successive extractions with 500 mL of EA at room temperature, followed by solvent evaporation under vacuum to yield 20.63 g of crude extract.

The crude extract was subjected to column chromatography over silica gel eluted with a gradient of petroleum ether–EA (*V*/*V*, 15∶1–0∶1) to obtain five main fractions (Fr. A–E). Fr. C (3.61 g) was subjected to silica gel column chromatography followed by eluting with a gradient of petroleum ether–EA (*V*/*V*, 5∶1–2∶1) to yield eight sub-fractions (Fr. C_1–C_8). Fr. C_2 (237.6 mg) was further purified by semi-preparative HPLC (MeCN–H_2O, 60∶40) to give **1** (10.5 mg, t_R 46.554 min) and **4** (16.4 mg, t_R 53.986 min). Fr. C_4 (342.1 mg) was separated using Sephadex LH-20 (CH_2Cl_2–MeOH, 1∶1), followed by semi-preparative HPLC (MeCN–H_2O, 49∶51) to obtain **3** (28.3 mg, t_R 49.543 min) and **2** (7.2 mg, t_R 52.080 min). Fr. C_6 (155.8 mg) was directly purified by semi-preparative HPLC (MeCN–H_2O, 68∶32) to afford **7** (35.9 mg, t_R 26.168 min). Fr. D (4.72 g) was subjected to silica gel column chromatography, followed by eluting with a gradient of petroleum ether–EA (*V*/*V*, 3∶1–1∶8) to yield nine subfractions (Fr.

D_1–D_9). Fr. D_5 (2.24 g) was chromatographed over Sephadex LH-20 (CH_2Cl_2–MeOH, 1∶1) to furnish six additional fractions (Fr. $D_{5\text{-}1}$–$D_{5\text{-}6}$), and Fr. $D_{5\text{-}3}$ (524.9 mg) was further purified by semi-preparative HPLC (MeCN–H_2O, 43∶57) to obtain **6** (13.6 mg, t_R 50.770 min), **5** (56.9 mg, t_R 73.646 min), and **8** (61.0 mg, t_R 83.070 min). Fr. D_7 (390.3 mg) was fractionated by Sephadex LH-20 (MeOH), followed by semi-preparative HPLC (MeCN–H_2O, 42∶58) to afford **9** (10.1 mg, t_R 21.425 min).

Templichalasin A (**1**): colorless crystals; $[\alpha]_D^{25}$ +237 (*c* 0.1, MeOH); UV (MeOH) λ_{max} (log ε) 203 (3.73) nm; IR (KBr) ν_{max} 3421, 2961, 2929, 2869, 2855, 1741, 1712, 1686 cm^{-1}; ECD (MeOH) λ_{max} ($\Delta\varepsilon$) 205 (+15.53), 231 (−2.51), 315 (−1.00) nm; ^1H and ^{13}C NMR data (Tables 1 and 2); (+)-HR-ESI-MS *m/z* 400.2512 $[M + H]^+$, 799.4936 $[2M + H]^+$.

Templichalasin B (**2**): white amorphous powder; $[\alpha]_D^{25}$ −81 (*c* 0.1, MeOH); UV (MeOH) λ_{max} (log ε) 203 (3.98) nm; IR (KBr) ν_{max} 3432, 2958, 2929, 2868, 2855, 1713, 1686, 1639 cm^{-1}; ECD (MeOH) λ_{max} ($\Delta\varepsilon$) 211 (+1.00), 243 (+1.66), 297 (−0.27), 332 (−0.11) nm; ^1H and ^{13}C NMR data (Tables 1 and 2); (+)-HR-ESI-MS *m/z* 400.2519 $[M + H]^+$, 799.4926 $[2M + H]^+$.

Templichalasin C (**3**): white amorphous powder; $[\alpha]_D^{25}$ +57 (*c* 0.1, MeOH); UV (MeOH) λ_{max} (log ε) 204 (4.04) nm; IR (KBr) ν_{max} 3430, 2960, 2928, 2868, 2855, 1714, 1687 cm^{-1}; ECD (MeOH) λ_{max} ($\Delta\varepsilon$) 242 (+1.52), 292 (−0.94) nm; ^1H and ^{13}C NMR data (Tables 1 and 2); (+)-HR-ESI-MS *m/z* 400.2510 $[M + H]^+$, 799.4927 $[2M + H]^+$.

6.4. X-ray crystal structure analysis

A single crystal of compound **1** was obtained in MeOH/H_2O solution *via* solvent volatilization. The crystallographic data for **1** (deposition No. CCDC2348049) has been deposited in the Cambridge Crystallographic Data Centre database.

Crystal data for **1**: $C_{24}H_{33}NO_4$ (*Mr* = 399.51 g·mol^{-1}), orthorhombic crystal, space group $P2_12_12$ (No. 18), *a* = 12.1165 (2) Å, *b* = 23.8546 (3) Å, *c* = 7.994 60 (10) Å, *V* = 2310.71 (6) $Å^3$, *Z* = 4, *T* = 99.99 (10) K, μ(Cu Kα) = 0.618 mm^{-1}, D_{calc} = 1.148 g·cm^{-3}, 53 345 reflections measured (7.412° ≤ 2Θ ≤ 148.492°), 4654 unique (R_{int} = 0.1131, R_{sigma} = 0.0345) which were used in all calculations. The final R_1 was 0.0652 [I > 2σ(I)] and wR_2 was 0.1756 (all data), Flack parameter = −0.18 (11).

6.5. ECD calculations

Conformational searches were performed using the GMMX program with MMFF94 force field. The conformers within 3 kcal·mol^{-1} of the lowest energy structure were selected for further density functional theory (DFT) calculations in the gas phase at the B3LYP-D3(BJ)/6-31G(d) level. The stability of all conformers was confirmed by the absence of imaginary frequencies in vibrational frequency calculations, conducted at the same level using Gaussian 16 software. Frequency calculations at 298.15 K were performed to obtain thermal corrections to Gibbs energies. Single-point energies were calculated at the (U)ωB97X-D/def2-QZVPP level, along with the SMD solvation model using the experimental solvent by the ORCA program system. The population distribution of each conformer was calculated by Boltzmann distribution based on Gibbs free energy with the isostat program. Conformers with a Boltzmann-weighted distribution exceeding 90% were selected for time-dependent density functional theory (TDDFT) calculations at the B3LYP/6-311++G(2d, p) level in methanol, applying the IEFPCM solvation model for methanol. These calculations considered 40 excited states for each conformer. Electronic transitions were modeled as Gaussian curves, with each peak having a full width at half maximum (FWHM) of 0.5 eV. The final calculated ECD spectra were then generated by Boltzmann-weighting.

6.6. Acid-mediated transformation of compound **4**

Samples of **4** (50 μg) were exposed for 24 h with (i) 1%, 10%, and 30% TFA in MeOH (200 μL) or (ii) 1%, 10%, and 30% TFA in H_2O (200 μL) at room temperature. Subsequently, the reaction mixtures were concentrated to dryness using a vacuum centrifugal concentrator (Beijing JM Technology, China) and redissolved in MeOH (200 μL) prior to LC-HRMS analysis.

6.7. Biological evaluation

6.7.1. Cell, virus, and tested compounds

Human laryngeal carcinoma cells (Hep-2), purchased from China Center for Type Culture Collection (CCTCC), were maintained in Dulbecco's modified Eagle's medium (DMEM, Gibco), supplemented with 10% fetal bovine serum (FBS, Gibco), 100 U·mL^{-1} of penicillin and streptomycin, and 2 mmol·L^{-1} L-glutamine. Live CVB3 strain was generously provided by Prof. Ying Zhu from the State Key Laboratory of Virology, College of Life Sciences, Wuhan University, China, and propagated in the Hep-2 cells. Viral titers were determined using the standard median tissue culture infective dose ($TCID_{50}$) [20]. Ribavirin, as a positive control, was purchased from Sigma Chemical Co. Stock solutions of drugs were prepared in dimethyl sulfoxide (DMSO) at a final concentration of 0.1% and diluted with maintenance medium (MM) comprising DMEM with 2% FBS.

6.7.2. Cytotoxicity assays

The cytotoxicity of compounds **1**–**9** against Hep2 cells was evaluated using the 3-(4,5-dimethylthiazol-2-yl)-2,5-diphenyl tetrazolium bromide (MTT) assay [21], a widely employed colorimetric method for evaluating cell viability and proliferation. Initially, Hep2 cells were seeded in 96-well plates and allowed to adhere overnight. Subsequently, serial dilutions of compounds **1**–**9** were prepared in a cell culture medium to achieve a range of concentrations. The cells were then treated with these compound solutions for 48 h, followed by removing the medium and addition of MTT. The cells were further incubated for 4 h at 37 °C to allow for the formation of formazan crystals by metabolically active cells. After incubation, the formazan crystals were solubilized using DMSO, and the absorbance was measured at 492 nm (OD 492) using a microplate reader (Thermo Scientific, MK3). The absorbance values obtained were directly proportional to the number of viable cells present in each well, enabling the determination of cytotoxic effects induced by compounds **1**–**9**. The 50% cell cytotoxic concentration (CC_{50}) of the compounds was calculated using a statistical package for the social sciences (SPSS) software. These experiments were conducted in triplicate to ensure statistical robustness and reproducibility of the results.

6.7.3. Antiviral assays and SI

The antiviral activities of compounds **1**–**9** against CVB3 were evaluated through *in vitro* cell-based assays. Initially, Hep2 cells were infected with 100 $TCID_{50}$ of CVB3 for 1.5 h at 37 °C. Then, the infected cells were exposed to various concentrations of compounds **1**–**9** and incubated at 37 °C, 5% CO_2, for 48 h. After incubation, the inhibition of virus-induced CPEs in acutely infected Hep-2 cells was recorded microscopically. The cell viability of Hep2 was determined using MTT assays. The concentration for each test compound was determined based on achieving 50% protection from virus-induced cytopathogenicity (EC_{50}). The SI was calculated as the ratio of CC_{50}/EC_{50}. Each experiment was conducted in triplicate and repeated independently at least three times.

6.7.4. Progeny virus yield and titration

Hep-2 cells were seeded in 24-well plates and infected with 100 $TCID_{50}$ of CVB3. Following 48 h of incubation with either spe-

cific concentrations of compounds or no treatment, culture media and cell lysates were collected after freeze-thaw cycles and subjected to virus titration. Serial 10-fold dilutions of viral suspensions in maintenance medium (MM) were used to inoculate Hep-2 cells in a 96-well plate. After 1.5 h of incubation at 37 °C in 5% CO_2, the unbound virus was removed by washing, and the MM was replenished. CPEs were monitored in infected cells after 2 days, and virus titers were calculated using the Reed–Muench method [20].

Funding

This work was supported by the National Natural Science Foundation of China (Nos. 31972852, 32371496, and 81903527) and the Key Project at Central Government Level: the Ability Establishment of Sustainable Use for Valuable Chinese Medicine Resources (No. 2060302).

Availability of supporting information

Supporting information for this work is available upon request from the corresponding authors *via* E-mail.

Declaration of interest

The authors declare no competing financial interest.

References

1 Massilamany C, Gangaplara A, Reddy J. Intricacies of cardiac damage in coxsackievirus B3 infection: implications for therapy. *Int J Cardiol*. 2014;177(2):330-339. https://doi.org/10.1016/j.ijcard.2014.09.136.
2 Huber S, Ramsingh AI. Coxsackievirus-induced pancreatitis. *Viral Immunol*. 2004;17(3):358-369. https://doi.org/10.1089/vim.2004.17.358.
3 Daley AJ, Isaacs D, Dwyer DE, et al. A cluster of cases of neonatal coxsackievirus B meningitis and myocarditis. *J Paediatr Child H*. 1998;34(2):196-198. https://doi.org/10.1046/j.1440-1754.1998.00176.x.
4 Han JY, Jeong HI, Park CW, et al. Cholic acid attenuates ER stress-induced cell death in coxsackievirus-B3 infection. *J Microbiol Biotechnol*. 2018;28(1):109-114. https://doi.org/10.4014/jmb.1708.08009.
5 Kim BK, Kim JH, Kim NR, et al. Development of anti-coxsackievirus agents targeting 3C protease. *Bioorg Med Chem Lett*. 2012;22(22):6952-6956. https://doi.org/10.1016/j.bmcl.2012.08.120.
6 Thibaut HJ, De Palma AM, Neyts J. Combating enterovirus replication: state-of-the-art on antiviral research. *Biochem Pharmacol*. 2012;83(2):185-192. https://doi.org/10.1016/j.bcp.2011.08.016.
7 El-Hawary SS, Moawad AS, Bahr HS, et al. Natural product diversity from the endophytic fungi of the genus *Aspergillus*. *RSC Adv*. 2020;10(37):22058-22079. https://doi.org/10.1039/D0RA04290K.
8 Hagag A, Abdelwahab MF, Abd El-Kader AM, et al. The endophytic *Aspergillus* strains: a bountiful source of natural products. *J Appl Microbiol*. 2022;132(6):4150-4169. https://doi.org/10.1111/jam.15489.
9 Zhu H, Chen C, Tong Q, et al. Progress in the chemistry of cytochalasans. *Prog Chem Org Nat Prod*. 2021;114:1-134. https://doi.org/10.1007/978-3-030-59444-2_1.
10 Chen R, Guo LJ, Li XD, et al. Phomopsischalins A–C, polycyclic-fused cytochalasins from the endophytic fungus *Phomopsis* sp. shj2 and their abilities to induce lysosomal function. *Org Chem Front*. 2023;10(9):2218-2225. https://doi.org/10.1039/D3QO00252G.
11 Zhang JM, Liu X, Wei Q, et al. Berberine bridge enzyme-like oxidase-catalysed double bond isomerization acts as the pathway switch in cytochalasin synthesis. *Nat Commun*. 2022;13(1):225. https://doi.org/10.1038/s41467-021-27931-z.
12 Shang Z, Raju R, Salim AA, et al. Cytochalasins from an Australian marine sediment-derived *Phomopsis* sp. (CMB-M0042F): acid-mediated intramolecular cycloadditions enhance chemical diversity. *J Org Chem*. 2017;82(18):9704-9709. https://doi.org/10.1021/acs.joc.7b01793.
13 Kemkuignou BM, Lambert C, Schmidt K, et al. Unreported cytochalasins from an acid-mediated transformation of cytochalasin J isolated from *Diaporthe cf. ueckeri*. *Fitoterapia*. 2023;166:105434. https://doi.org/10.1016/j.fitote.2023.105434.
14 Scherlach K, Boettger D, Remme N, et al. The chemistry and biology of cytochalasans. *Nat Prod Rep*. 2010;27(6):869-886. https://doi.org/10.1039/b903913a.
15 Wei G, Tan D, Chen C, et al. Flavichalasines A–M, cytochalasan alkaloids from *Aspergillus flavipes*. *Sci Rep*. 2017;7:42434. https://doi.org/10.1038/srep42434.
16 Keller-Schierlein W, Kupfer E. Stoffwechselprodukte von mikroorganismen. 186. mitteilung. über die aspochalasine A, B, C und D. *Helv Chim Acta*. 1979;62(5):1501-1524. https://doi.org/10.1002/hlca.19790620516.
17 Chen L, Liu YT, Song B, et al. Stereochemical determination of new cytochalasans from the plant endophytic fungus *Trichoderma gamsii*. *Fitoterapia*. 2014;96:115-122. https://doi.org/10.1016/j.fitote.2014.04.009.
18 Wu Z, Zhang X, Al Anbari WH, et al. Amiaspochalasins A–H, undescribed aspochalasins with a C-21 ester carbonyl from *Aspergillus micronesiensis*. *J Org Chem*. 2019;84(9):5483-5491. https://doi.org/10.1021/acs.joc.9b00440.
19 Ding G, Chen L, Chen A, et al. Trichalasins C and D from the plant endophytic fungus *Trichoderma gamsii*. *Fitoterapia*. 2012;83(3):541-544. https://doi.org/10.1016/j.fitote.2011.12.021.
20 Reed LJ, Muench H. A simple method of estimating fifty percent endpoints. *Am J Epidemiol*. 1938;27(3):493-497. https://doi.org/10.1093/oxfordjournals.aje.a118408.
21 Kumar P, Nagarajan A, Uchil PD. Analysis of cell viability by the MTT assay. *Cold Spring Harb Protoc*. 2018;2018(6):95505. https://doi.org/10.1101/pdb.prot095505.